In Situ Control of the Oxide Layer on Thermally Evaporated Titanium and Lysozyme Adsorption by Means of Electrochemical Quartz Crystal Microbalance with Dissipation

Isabel Van De Keere,*,† Sofia Svedhem,‡ Hans Högberg,§ Jean Vereecken,† Bengt Kasemo,‡ and Annick Hubin†

Research Group Electrochemical and Surface Engineering, Department of Materials and Chemistry, Vrije Universiteit Brussel, Pleinlaan 2, Brussels B-1050, Belgium, Biological Physics Group, Department of Applied Physics, Chalmers University of Technology, Fysikgränd 3, Göteborg SE-412 96, Sweden, and Thin Film Physics Division, Department of Physics (IFM), Linköping University, Linköping SE-581 83, Sweden

ABSTRACT Electrochemical (EC) quartz crystal microbalance with dissipation monitoring (ECQCM-D) is a new and powerful technique for the in situ study of adsorption phenomena, e.g., as a function of the potential of the substrate. When titanium (Ti) is employed as the substrate, its oxidation behavior needs to be taken into account. Ti is always covered with a native oxide layer that can grow by, e.g., thermal oxidation or under anodic polarization. For biomolecular adsorption studies on oxidized Ti under applied potential, a stable oxide layer is desired in order to be able to distinguish the adsorption phenomena and the oxide growth. Therefore, the oxidation of thermally evaporated Ti films was investigated in phosphate-buffered saline by means of ECQCM-D, using a specially designed EC flow cell. Upon stepping the potential applied to Ti up to 2.6 V vs standard hydrogen electrode (SHE), a fast increase of the mass was observed initially for each potential step, evolving slowly to an asymptotic mass change after several hours. The oxide layer thickness increased as a quasi-linear function of the oxidation potential for potentials up to 1.8 V vs SHE. The growth rate of the oxide was around 2.5−3 nm/V. No changes in the dissipation shift were observed for potentials up to 1.8 V vs SHE. The composition of the oxide layer was analyzed by X-ray photoelectron spectroscopy (XPS). It was mainly composed of TiO_2, with a small percentage of suboxides (TiO and Ti_2O_3) primarily at the inner metal/oxide interface. The amount of TiO_2 increased, and that of TiO and Ti_2O_3 decreased, with increasing oxidation potential. For each oxidation potential, the calculated thickness obtained from ECQCM-D correlated well with the thickness obtained by XPS depth profiling. A procedure to prepare Ti samples with a stable oxide layer was successfully established for investigations on the influence of an electric field on the adsorption of biomolecules. As such, the effect of an applied potential on the adsorption behavior of lysozyme on oxidized Ti was investigated. It was observed that the adsorption of lysozyme on oxidized Ti was not influenced by the applied potential.

KEYWORDS: ECQCM-D • titanium • oxide film stability • electrochemical oxidation • XPS • biomolecules

INTRODUCTION

Titanium (Ti) is frequently used as a biomaterial in orthopaedics and cardiovascular devices (1). The metal is covered with a native oxide layer of a few nanometers (2), which contributes to the high biocompatibility of Ti implants (3). A cascade of events occurs on the surface of a biomaterial when it is implanted in the human body. Proteins adsorb within seconds, followed by cells interacting with the already adsorbed proteins rather than directly with the surface of the implant itself (4−6). One of the surface properties of a biomaterial that plays an impor-

tant role in the electrostatic interaction with biomolecules is its surface charge. The surface charge of a biomaterial depends mostly on the type of surface oxide, the pH, and the electrochemical reactions occurring at the surface because they determine the potential. By variation of the potential of Ti, the surface charge of Ti changes, and electrostatic interactions are likely to be influenced (7−9). The understanding of these interactions is critical for the development of new biomaterials and implants (10−12). By a combination of in situ sensing techniques with electrochemical methods, new information is obtained about surface and interfacial processes. The quartz crystal microbalance (QCM) technique is a well-established technique for monitoring of the mass (13, 14) and film thickness in coating equipment in vacuum and for investigations of gas adsorption and surface reactions in the monolayer range, via changes in the resonant frequency, f. More recently, the technique has also been proven valuable for studying surface-

related processes in liquids (13, 14), including protein adsorption (15−19). A recent extension of the technique, called QCM-D, to simultaneously measure changes in the frequency, Δf, and in the energy dissipation, ΔD, of the QCM (20, 21) provides new insight into e.g., protein adsorption processes (17−19) as well as other surface-related processes (22−24). The energy dissipation factor, D, can be defined as $D = E_{dissipated}/2\pi E_{stored}$, where $E_{dissipated}$ is the energy dissipated during one period of oscillation and E_{stored} is the energy stored in the oscillating system (25). It is, in the current case, measured by recording the response of a freely oscillating crystal that has been vibrated at its resonance frequency. By measurement of the dissipation, ΔD, information about the viscoelastic properties of the adsorbed layers can be obtained. From the dissipation shift ΔD and (Δf, ΔD) plots, structural information can be obtained about a deposited protein film. The slope of (Δf, ΔD) plots gives information about viscoelastic changes in the protein film as a function of the coverage and/or added mass. When several slopes are observed for certain processes, this might indicate that conformational changes or changes in the hydrated state of the film have occurred. In comparison with optical waveguide lightmode spectroscopy (9, 26−29) and ellipsometry (30, 31), one advantage of the QCM technique is that the surface material can be fairly freely chosen without having to consider special properties such as optical transparency or reflectivity, as long as the preferred material can be deposited as a thin (up to micrometer thickness) film onto the sensor crystals. One property of the method that sometimes is an advantage, and sometimes a complication, is that the method measures coupled water. The advantage comes because the amount of coupled water can be measured when combined QCM with dissipation is combined with water-insensitive techniques like surface plasmon resonance or reflectometry (32).

It has recently become possible to carry out combined QCM-D and electrochemical (EC) measurements using a specially designed flow cell. ECQCM has existed for many years (33−41), even as commercial instruments, but not ECQCM-D. This combination is valuable for adsorption studies under the influence of external fields (34) and/or when one wants to change in situ the oxide layer thickness (35−41). Fleming et al. (42) have employed ECQCM-D to study the adsorption of azurin on a gold electrode modified with an alkanethiol self-assembled monolayer. In their investigation, the adsorption of azurin was monitored by QCM-D, after which cyclic voltammetry was performed, using a commercially available electrochemistry module.

The long-term goal of the current study is to gain a better understanding of the adsorption mechanism of biomolecules, such as proteins and lipids, on implant surfaces, and more specifically under the influence of an electric field. Therefore, it is important to investigate in real time how the surface characteristics affect the amount of adsorbed biomolecules and surface-induced conformational changes, which can be achieved by means of ECQCM-D. A difficulty arises upon using Ti compared to model substrates such as
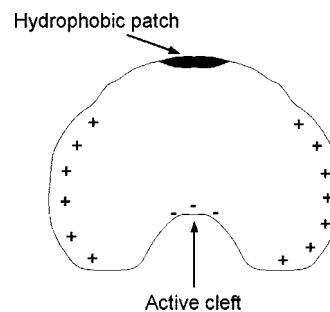

FIGURE 1. Molecular structure of HEL, according to Gölander et al. (44).

gold, because the surface of Ti is always covered with a native oxide layer, which may grow upon application of a potential to the Ti surface. Because adsorption phenomena need to be distinguished from the oxide growth upon application of a potential to the surface, a stable oxide layer is desired before investigating the interaction of biomolecules with Ti. The QCM-D technique, in principle, offers the possibility of first measuring the oxide growth by in situ (anodic) oxidation and then performing biomolecule adsorption experiments in the same cell, with or without an applied external electric field. This is one type of study we are aiming at here. Alternatively, if the oxide growth occurs in parallel with biomolecular adsorption, one can calibrate the former, and subtract it, by separate measurements without biomolecules.

The aim of the present study is to understand the oxidation behavior of Ti in biologically relevant buffer solutions by means of ECQCM-D and to prepare Ti surfaces such that a stable oxide layer, i.e., no later growth, is obtained for adsorption studies under the influence of an applied potential. The goal is to obtain quantitative information on the growth behavior and the thickness of the titanium oxide layer with ECQCM-D. The calculated thickness from EC-QCM-D will be correlated with depth profiles obtained by X-ray photoelectron spectroscopy (XPS). From XPS data, the chemical composition of the electrochemically grown titanium oxide layer at several oxidation potentials will be analyzed.

Once a stable oxide layer is obtained, the adsorption of hen egg white lysozyme (HEL) under the influence of an electric field will be investigated on the titanium oxide surfaces by means of ECQCM-D. HEL is one of the best known proteins. In the human body, lysozyme is abundant in tears and saliva. Lysozyme catalyzes the hydrolysis of heterogeneous polysaccharides, which consist of *N*-acetylmuramic and *N*-acetylglucosamine (43). This type of polysaccharide is present in the cell walls of Gram-positive bacteria, and its hydrolysis leads to the destruction of the bacteria. HEL is a small compact protein with a molecular weight of 14.4 kDa and an isoelectric point p*I* of 10.5 (8). The structure of HEL is shown in Figure 1 (44). The aim is to obtain quantitative information about the adsorbed mass per unit area of HEL with ECQCM-D. By measurement of the dissipation shift, the goal is to gain insight in the viscoelastic properties of the adsorbed protein film.

EXPERIMENTAL SECTION

Chemicals. Phosphate-buffered saline (PBS; 0.01 M phosphate buffer, 0.0027 M potassium chloride, 0.137 M sodium chloride, pH 7.4, at 22 °C; Sigma-Aldrich) was used as the electrolyte. Water was purified and deionized (resistivity > 18 MΩ/cm) using a MilliQ unit (Millipore France, Molsheim, France).

Proteins. Hen egg white lysozyme (HEL, L6876), with a protein content of more than 90%, was purchased in lyophylized form from Sigma-Aldrich. The protein powder was dissolved in PBS at a concentration of 10 mg/mL. Stocks were frozen at −20 °C for storage. After thawing, the stock solution was diluted in PBS to final concentrations of 1 mg/mL. All of the measurements were performed at 22 °C.

Substrates. The QCM crystals were AT-cut quartz crystals with a fundamental resonant frequency of approximately 5 MHz. Custom-made crystals were provided by Q-Sense AB (Västra Frölunda, Sweden).

The excitation of an AT-cut quartz crystal is made possible by means of an applied voltage between two electrodes, one deposited on each side of the AT-cut crystal (45). A gold electrode was deposited on the bottom of the crystal. A Ti film was deposited on top of the crystal by means of thermal (electron-beam) evaporation at room temperature in vacuum (AVAC HVC-600, 10^{-6} mbar). Prior to deposition of Ti, the crystals were cleaned by means of an oxygen plasma treatment. The typical deposition rate was about 2.5−3 Å/s, and the deposited thickness of Ti on top of the QCM crystal was about 300 nm. A schematic of a Ti-coated QCM crystal is shown in Figure 2a.

Combined ECQCM-D Setup. The ECQM-D measurements were performed with an E4 instrument from Q-Sense AB equipped with a newly designed flow module for electrochemical purposes (see Figure 2b). The flow module was connected to a Gamry potentiostat (PCI4750, series G750; controlled by the *Gamry Framework* software package). Ti-coated QCM crystals were mounted in the flow module, and the Ti film deposited onto the QCM crystal served at the same time as one of the electrodes for QCM-D and as the working electrode in the electrochemical measurements. Before the crystals were mounted, they were rinsed with water, dried with nitrogen gas, and treated in a UV−ozone chamber for 30 min. The inner volume of the flow cell was approximately 90 μL. The working solution was sucked into the flow cell through the liquid inlet by means of a peristaltic pump. The solution first flowed through a Peltier element (not shown in Figure 2b) before entering the inner cell volume through the inlet hole in the platinum (Pt) counter electrode disk. The purpose of the Peltier element is to heat up or cool down the solution and to stabilize its temperature prior to its arrival in the inner cell volume. The solution flowed out of the cell chamber through the outlet hole in the Pt counter electrode disk using a set flow rate chosen on the peristaltic pump. The experiments were performed at 22.0 ± 0.1 °C, under static conditions (no flow) for the oxidation of Ti and at a flow rate of 50 μL/min for the protein adsorption experiments. The geometric sensing area was 0.78 cm².

Chronoamperometric/potentiostatic experiments were conducted using a three-electrode setup. The Ti-coated crystal acted as the working electrode, a standard Ag/AgCl electrode (Schott Instruments, Scienceline B3420+) served as the reference electrode, and a Pt disk (Alfa Aesar, Johnson Matthey) was used as the counter electrode. The reference electrode was placed in a custom-made Teflon holder filled with the working solution and in connection with the liquid outlet channel of the flow module. An O-ring surrounding the reference electrode at the entrance of the Teflon holder was used to seal off the holder. The counter electrode was positioned parallel to the working electrode. All potentials reported in this paper are expressed versus standard hydrogen electrode (SHE). The potential measured for the Ag/AgCl reference electrode in a saturated KCl solution was 200 mV vs SHE. The applied potentials in the potentiostatic experiments ranged between 0.6 and 2.6 V. Changes in the resonance frequency of the crystals during the experiments, Δf, were converted into a mass change at the interface, Δm, by means of the Sauerbrey equation (46), $\Delta m = -C\Delta f/n$, where n is the overtone number and C is the calibration constant determined by the physical properties of the crystal [$C = 17.7$ ng/(cm² Hz) for the quartz crystal used in this study]. The frequency shifts were normalized to the fundamental frequency by division with the overtone number $n = 9$.

XPS Analysis. The Ti surfaces were analyzed with the XPS instrument PHI 1600, using an acceleration voltage of 15 kV and a power of 300 W. X-ray Mg Kα radiation (1253.6 eV) was used. The sample was excited by X-rays over a spot area of approximately 0.8 mm diameter. Photoelectrons were detected with a hemispherical analyzer positioned at an angle of 45° with respect to the normal to the sample surface. Survey scan spectra were made at a pass energy of 58.7 and 0.5 eV energy steps, while for C 1s, O 1s, and Ti 2p individual high-resolution spectra were taken at a pass energy of 23.5 and 0.1 eV energy steps. After taking the surface spectra, depth profiling of the surface was performed. An Ar$^+$ ion beam with an energy of 4 keV at an incidence angle of 45° and a raster of 2 mm × 2 mm was used for ion sputtering. The sputtering rate was 3 nm/min as calibrated for Ta$_2$O$_5$. The sputter interval was 0.1 min. XPS concentration profiles were calculated using relative sensitivity factors from the manufacturer's handbook (47).

Data analysis of the XPS spectra and depth profiles was done by means of the PHI Multipak software package (version 8.0). The XPS spectra were background-subtracted using the nonlinear, iterative Shirley method (48) and fitted by a least-squares trial and error procedure with mixed Gaussian/Lorentzian peaks based on the method of Sherwood (48). The fitted signals were evaluated by determination of the peak position, height, width, and Gaussian/Lorentzian ratio (49, 50). The depth profiles were further analyzed by performing a linear least-squares fit for the different detected elements (51).

RESULTS

In the following, we describe first the electrochemically driven oxidation process at the surface of the thermally deposited Ti films, as monitored by ECQCM-D, and second the compositional characterization of the resulting oxide layers by XPS. Then we describe the adsorption behavior of HEL on the oxidized Ti surfaces under the influence of an applied potential, measured by means of ECQCM-D.

Electrochemically Driven Oxidation of Ti Films under an Applied Anodic Potential. After the Ti-coated QCM crystals were mounted in the electrochemical flow module, the QCM-D signal stabilized in PBS. However, because the QCM-D module was connected to a potentiostat (and appropriately grounded), the noise level of the dissipation shift was higher than what is generally expected for QCM-D experiments. Because of the higher noise levels induced by the coupling of the QCM-D with the electrochemical setup, it is mostly not possible to get a low-noise signal at lower frequencies. The ninth overtone quasialways behaved very well: its resonance peak was well resolved, and low-noise signals were detected. That is why the ninth overtone was chosen for all further analysis.

The open circuit potential (OCP) of the Ti-coated QCM crystal, covered with its native oxide and immersed in PBS, was approximately 0.2 V. The results from a typical oxidation experiment under an applied potential are
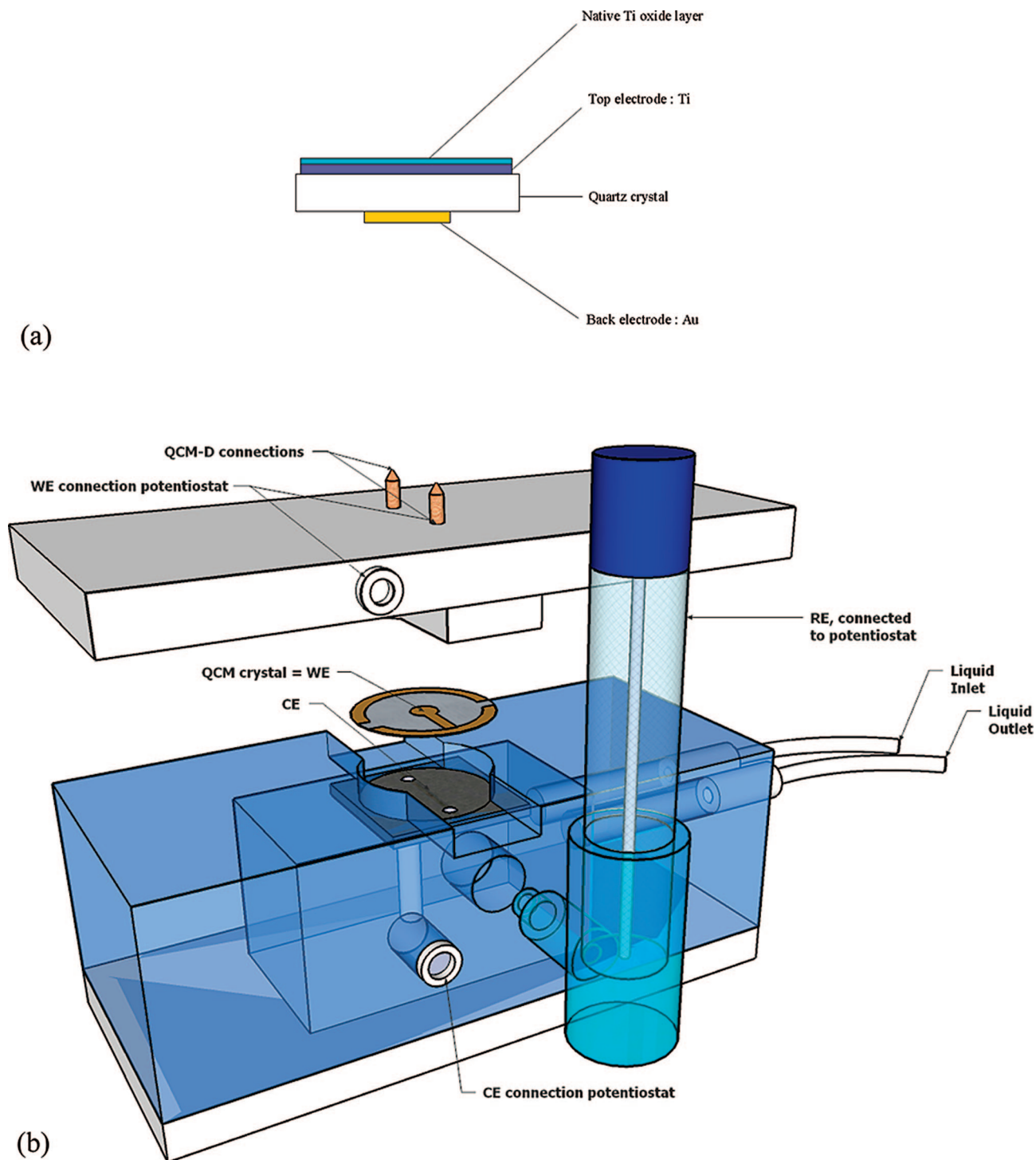
FIGURE 2. Schematic representation of (a) a Ti-coated QCM crystal (not to scale) and (b) the electrochemical flow module with the positioning of a QCM sensor. The solution flows into/out of the cell chamber through a small hole in the Pt counter electrode. The Ti-coated QCM crystal acts as the working (WE), electrode, an Ag/AgCl electrode serves as the reference electrode (RE), and a Pt disk is used as the counter electrode (CE).

shown in Figure 3, where the evolution of the frequency shift and the dissipation shift for the ninth overtone are plotted as a function of time for the investigated range of applied potentials, i.e., 0.6, 1, 1.8, and 2.6 V. The oxidation time per voltage step was 8 h. Upon stepping the potential to a higher value, a fast decrease of the frequency shift was observed initially, evolving to a stable level after several hours. This means that the oxide first grew rapidly and then

eventually stopped growing and reached an equilibrium state in qualitative agreement with published literature on anodic oxidation (52–56). The frequency shift per voltage step increased proportionally to the applied voltage for the range of applied potentials, going from 0.6 V up to 1.8 V. Within this range, no dissipation shifts were observed during the oxidation. However, upon a further increase of the applied potential to 2.6 V, the linear relation between the
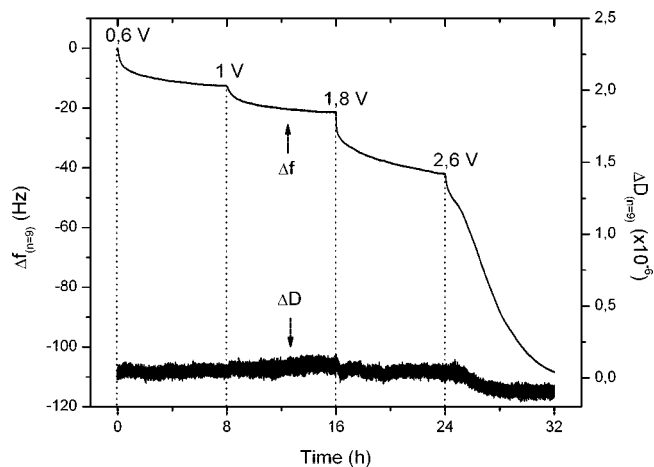
FIGURE 3. QCM-D frequency (Δf) and dissipation (ΔD) shifts showing the oxidation at the surface of a Ti-coated QCM crystal in PBS at four different anodic potentials. The potentials were each applied for 8 h. The frequency shifts were normalized to the fundamental frequency by division with the overtone number $n = 9$.
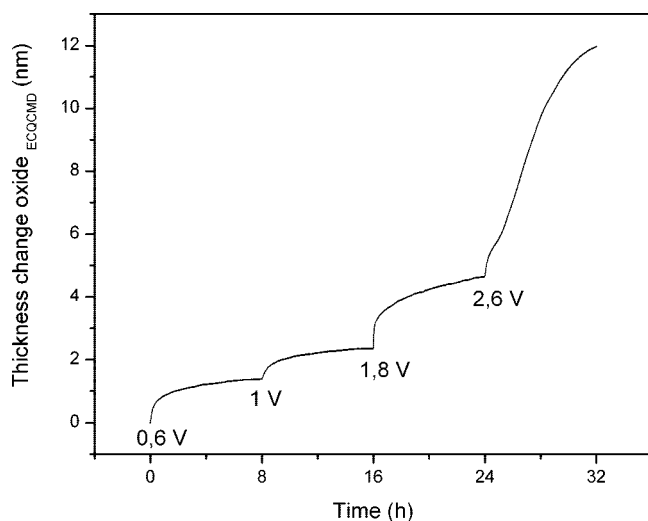

FIGURE 4. Oxide thickness change calculated by means of a QCM-D model based on the Sauerbrey equation during oxidation of a Ti-coated QCM crystal in PBS at four different anodic potentials. The potentials were each applied for 8 h.

applied potential and the frequency shift no longer held, and a large frequency shift was observed accompanied by a decrease in dissipation. Because the dissipation shift of the oxide growth was approximately 0 and thus much smaller than 10^{-5} (57), the Sauerbrey equation was valid. Therefore, the Sauerbrey equation, allowing translation of frequency shifts to mass uptake, was used to convert the measured frequency shifts to oxide film thickness, by assuming the formation of a rigid TiO_2 layer at the Ti surface, i.e., uptake of oxygen with the resulting composition of TiO_2. The density of a rigid TiO_2 layer is 4 g/cm^3. The calculated thickness is plotted in Figure 4.

High reproducibility of these results was obtained for a large series of crystals, prepared at different occasions. In Figure 5, the ECQCM-D thickness change of the oxide is plotted versus the applied potential for five Ti samples. A linear variation of the oxide film thickness with the applied potential was observed up to 1.8 V for all five Ti-coated QCM
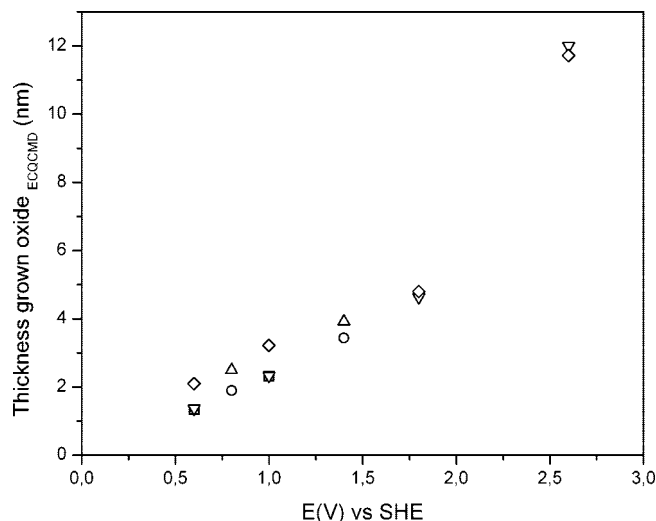

FIGURE 5. Oxide thickness changes calculated by means of a QCM-D model based on the Sauerbrey equation as a function of the applied potential for five Ti samples (each crystal is represented by its own symbol).

crystals. The growth rate of the oxide layer for the Ti-coated QCM crystals was determined to be 2.5 ± 0.1 nm/V. This growth rate is in accordance with measurements on bulk Ti performed by other techniques (7, 52−56). When the Ti-coated QCM crystals were oxidized at 2.6 V, a larger increase of the oxide thickness was detected. The initial linear relation between the thickness and voltage was obviously not valid anymore. This is at variance with other reports on Ti oxidation at much larger thicknesses (58, 59), and possible reasons will be discussed below.

An important observation for adsorption studies is that, upon application of an external potential near the OCP of Ti and lower than the earlier applied oxidation potential, the frequency shift and the dissipation shift were not changing. Thus, the oxide did not grow anymore due to a strong electrochemical irreversibility between the processes of titanium oxide formation and reduction.

Compositional Analysis of the Titanium Oxide Layers by XPS. Two regions with different oxidation behavior were observed in Figures 3−5. For oxidation potentials up to 1.8 V, a linear growth of the oxide layer as a function of the applied potential was observed without any change in dissipation, whereas for an oxidation potential of 2.6 V, this linear relation was not valid anymore and a decrease in dissipation was observed. XPS was used to investigate possible reasons for this difference in oxide growth. XPS measurements were therefore performed for two differently oxidized Ti-coated QCM crystals, oxidized at 1 and 2.6 V, one from each region. The properties of interest were the spectral features (what type of oxide) and a comparison between the obtained thickness changes from ECQCM-D measurements and the XPS depth profiles.

1. Surface Composition: XPS Survey Spectra. To determine the surface chemistry of the oxidized Ti layers, XPS analyses were performed on the Ti-coated quartz crystals before and after the electrochemical oxidation had been performed. Figure 6 shows the XPS survey scan
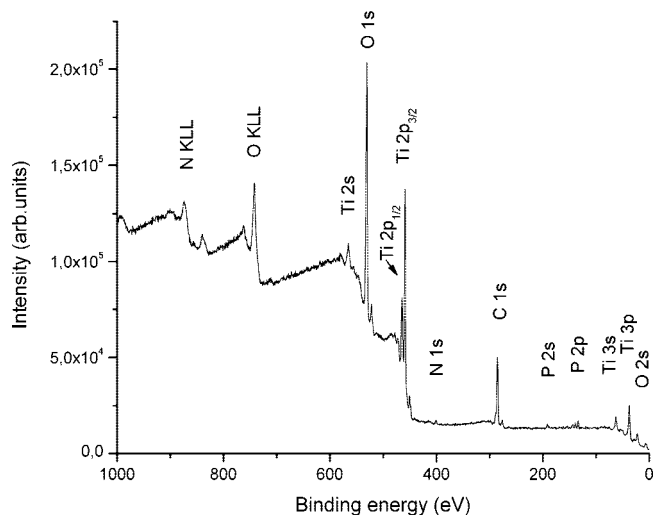
ACS APPLIED MATERIALS & INTERFACES

FIGURE 6. XPS survey scan spectrum of the electrochemically oxidized Ti surface at 1 V in PBS.

spectrum of a Ti surface oxidized at 1 V. Ti, C, O, and P peaks are present in the spectra. The Ti and O signals dominate the spectra, which indicates that the surface mainly consists of a titanium oxide layer. The C signal derives from the well-known inevitable contamination of oxidized Ti surfaces, when they have been exposed to ambient air (60). P was detected in small amounts. It is known from the literature that anodic oxidation can result in the incorporation of anions from the anodizing electrolyte in the bulk of the oxide layer. Lausmaa et al. (52, 61) observed the incorporation of S and P in the oxide film. The P peaks visible in Figure 6 disappeared after a short time of argon ion etching however, which showed that P was not present in the bulk of the oxide film. Most likely, P was present in the form of phosphate ions on the surface, which had been adsorbed from the electrolyte.

2. Surface Oxide Stoichiometry: High-Resolution XPS Spectra. The composition of the oxide layers was determined from high-resolution XPS spectra of Ti 2p. In parts a and b of Figure 7, the high-resolution spectra of the Ti 2p transition from the Ti surface, oxidized at 1 and 2.6 V, respectively, are given. The Ti 2p peak is composed of spin doublets, separated by 5.7 eV. For both spectra, the Ti $2p_{3/2}$ peak shows a large contribution at a binding energy of 459 ± 0.1 eV, corresponding to TiO_2 (52, 62–66). Smaller contributions to the Ti $2p_{3/2}$ peak were observed in both spectra at binding energies of 457.4 ± 0.1 and 454.3 ± 0.1 eV, which are attributed to the suboxides Ti_2O_3 and TiO, respectively (52, 62–64, 67–72). Accordingly, Ti $2p_{1/2}$ peaks were observed at binding energies of 464.9 ± 0.1 eV (TiO_2), 463.7 ± 0.1 eV (Ti_2O_3), and 460.4 ± 0.1 eV (TiO). For both oxide films, oxidized at either 1 or 2.6 V, three components, i.e., TiO_2, Ti_2O_3, and TiO, were thus present in the oxide layer. For the Ti surface oxidized at 2.6 V, the TiO_2 peak dominated the spectra and the contributions of Ti_2O_3 and TiO were smaller than in the spectrum at 1 V, as quantified in Table 1. The intensities of the suboxides, i.e., TiO and Ti_2O_3, thus decreased by an increase in the oxidation potential, whereas that of the oxide TiO_2 increased. Angular-dependent studies of thin titanium oxide films (ca. 10 Å) (73)
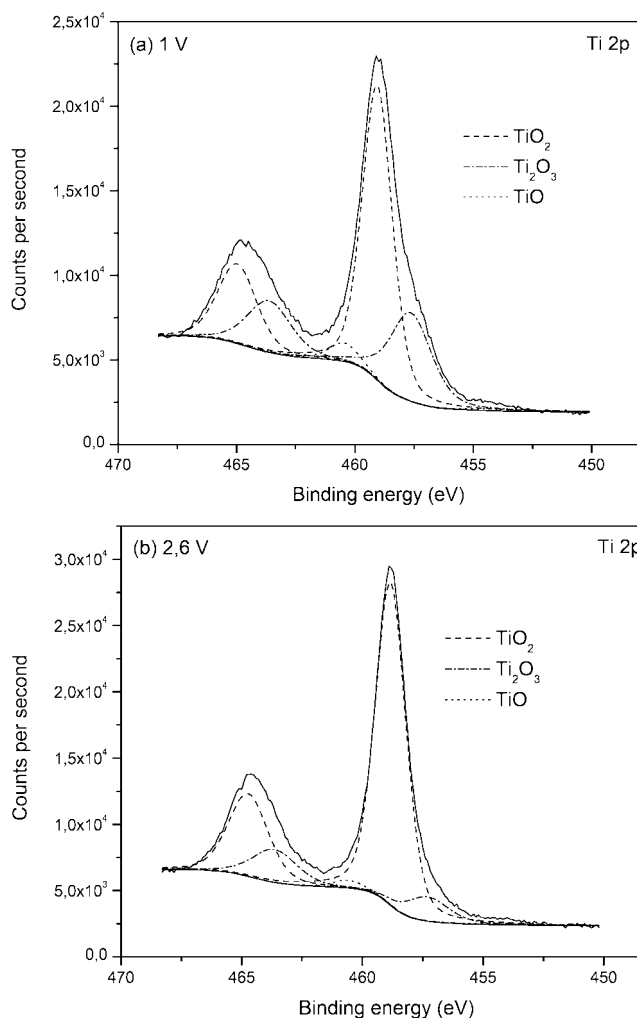

FIGURE 7. Deconvoluted Ti 2p high-resolution spectrum of the electrochemically oxidized Ti surface recorded at 1 V (a) and 2.6 V (b) in PBS. The experimental spectrum is given as a solid line, and component peaks of the fitted spectrum are represented by dashed lines.

Table 1. Summary of the Obtained Results for the Oxide Layer Thickness and Chemical Composition at 1 and 2.6 V by Means of ECQCM-D and XPS

applied potential (V)	ECQCM-D oxide film thickness changes	XPS oxide film thickness (nm)	XPS peak area (%)		
			TiO_2	Ti_2O_3	TiO
1	2.3 ± 0.1	7.8 ± 0.1	64	33	3
2.6	12.0 ± 0.1	18.3 ± 0.1	82	16	2

have established that the lower oxidation states Ti^{2+} and Ti^{3+} are formed preferentially at the metal–oxide interface, whereas Ti^{4+} species are dominant at the oxide–gas interface. Thus, the intensities from the two suboxides were reduced because of their location at the metal–oxide interface and the exponential decay of their XPS signatures with increasing oxide thickness (63, 71, 73).

3. Surface Oxide Depth Profiling. Figure 8 shows an overlay of the XPS depth profiles for Ti, O, and C from two Ti surfaces, one oxidized at 1 V and the other one at 2.6 V. By means of a linear least-squares fitting (51), the analysis and interpretation of the depth profiles were greatly
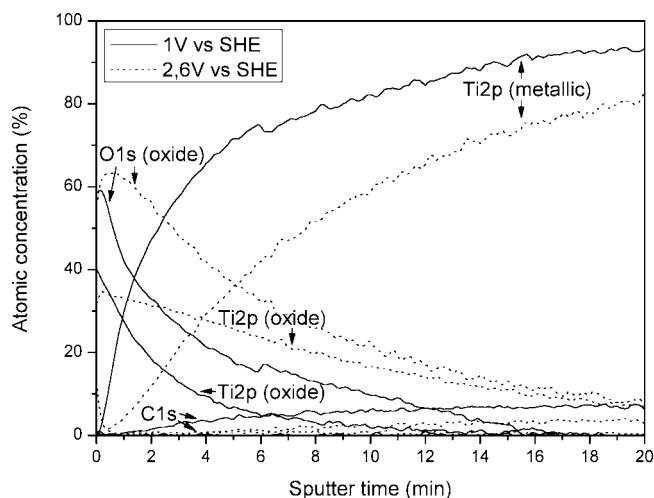
FIGURE 8. XPS depth profiles of titanium oxide films grown respectively at 1 and 2.6 V in PBS.

enhanced. The Ti (oxide) and O (oxide) signals decrease from a maximum at the surface to a noise level in the bulk of the metal film, and the Ti (metallic) signals increase to a maximum in the bulk, which are typical profiles of a thin oxide film. The depth/sputter time at which the O (oxide) signal has decreased to 50 % of its maximum value at the surface, is used as an estimation of the oxide thickness (60). When these times are compared for the two surfaces, one can deduce that the oxide thickness increases with increasing anodic potential, as expected. The absolute XPS-derived thickness of the oxide layer was estimated by multiplying the sputter time, at which the O (oxide) signal has decreased to 50 % of its maximum value at the surface, with the sputter rate of Ta_2O_5 determined with XPS under the same experimental conditions. The thickness of the oxide after oxidation at 1 V is 7.8 ± 0.1 nm, whereas for 2.6 V, the thickness is 18.3 ± 0.1 nm, as summarized in Table 1. The values determined from the ECQCM-D results in Table 1 represent the thickness changes of the oxide upon oxidation relative to the native oxide layer thickness, whereas the values determined with XPS represent the total oxide thickness (=native oxide layer thickness + thickness change of the oxide upon oxidation). Upon comparison of the XPS and ECQCM-D results for 1 and 2.6 V in Table 1, the difference between their ECQCM-D-derived oxide thickness changes after oxidation is 9.7 ± 0.1 nm, while the difference between their absolute XPS-derived thicknesses is 10.5 ± 0.1 nm. Thus, the oxide growth measured with ECQCM-D and XPS is in good agreement. The thickness of the native oxide layer is estimated to be around 6 nm. This value is in good agreement with previous XPS measurements of native titanium oxide films (52, 74).

It was found that the C signal for both Ti surfaces consisted of two components after a linear least-squares fit. One component dropped to zero in less than 30 s of Ar^+ ion etching. Its presence was attributed to carbon contamination at the surface after exposure to air (60). The second component was not present at the interface before ion sputtering but appeared after approximately 1 and 7 min of ion etching for 1 and 2.6 V, respectively. The presence of this compo-
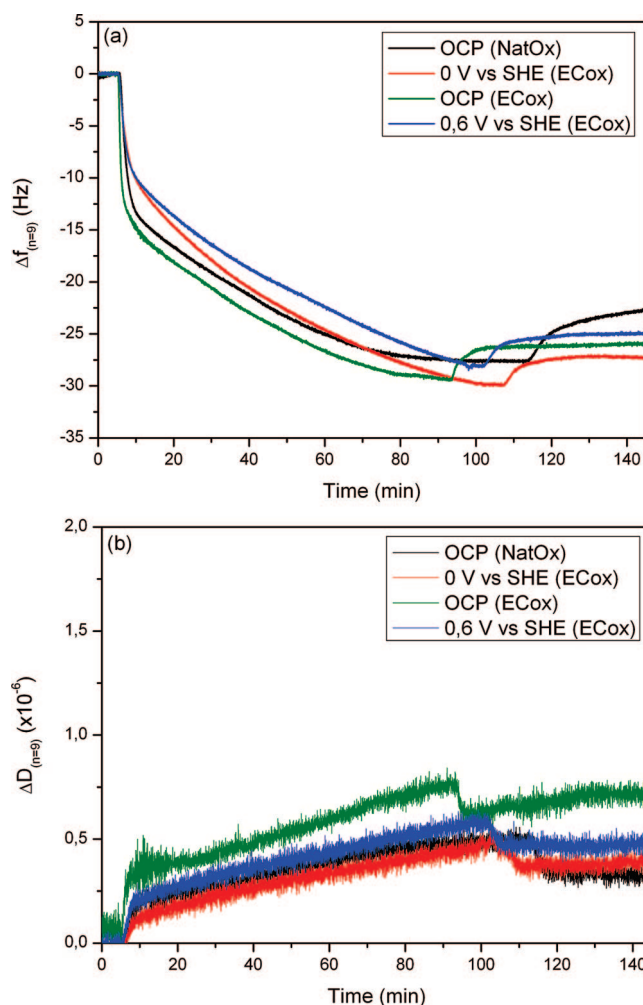

FIGURE 9. Comparison between the detected changes in Δf (a) and ΔD (b) for the adsorption of 1 mg/mL of HEL on Ti-coated QCM crystals covered with either their native oxides (NatOx) at OCP or their electrochemically grown oxides (ECox) at OCP, 0 and 0.6 V. The frequency shifts were normalized to the fundamental frequency by division with the overtone number $n = 9$.

nent is due to the formation of carbides at the interface during ion sputtering. Nonideal (contaminated) vacuum conditions in the XPS instrument are the main cause for the formation of carbides (64).

Adsorption of Lysozyme onto Ti under an Applied Potential. The adsorption of 1 mg/mL of HEL in PBS was investigated on Ti-coated QCM crystals covered with either their native oxides at OCP (approximately 0.2 V) or with their electrochemically grown oxides at OCP (approximately 0.25 V), 0 and 0.6 V. In Figure 9, the changes in frequency $\Delta f_{n=9}$ and dissipation $\Delta D_{n=9}$ upon adsorption of 1 mg/mL of HEL on both types of oxides and for different applied potentials are shown. An initial rapid decrease in the frequency, and thus a rapid increase of sensed mass, was followed by a slower decrease of the frequency, and thus a slower increase of sensed mass, reaching an equilibrium state after approximately 100 min. No significant differences were observed between the frequency shifts of HEL at saturation on the native titanium oxide at OCP and the frequency shifts of HEL at saturation on the electrochemically grown titanium oxide at OCP, 0 and 0.6 V, as shown

Table 2. Changes in Frequency and Dissipation at the Ninth Overtone, as Well as Average Adsorbed Amounts per Unit Area Γ of 1 mg/mL of HEL after Approximately 80 min of Adsorption on Ti-Coated QCM Crystals Covered with Either Their Native Oxides (NatOx) at OCP or Their Electrochemically Grown Oxides (ECox) at OCP, 0 and 0.6 V[a]

applied potential (V)	$\Delta f_{n=9}$ (Hz)	$\Delta D_{n=9}$ (10^{-6})	$\Gamma_{Sauerbrey}$ (ng/cm^2)
OCP (NatOx) ≈ 0.2 V	−27.3 ± 0.1	0.47 ± 0.01	483 ± 2
0 V (ECox)	−28.3 ± 0.1	0.43 ± 0.01	501 ± 2
OCP (ECox) ≈ 0.25 V	−29.1 ± 0.1	0.70 ± 0.01	515 ± 2
0.6 V (ECox)	−26.5 ± 0.1	0.52 ± 0.01	469 ± 2

[a] The adsorbed amounts per unit area were calculated by means of the Sauerbrey equation.

in Figure 9a. Also, no significant differences were observed between the dissipation shifts, as shown in Figure 9b. Table 2 sums up the frequency and dissipation shifts at the ninth overtone for both oxide types and the different applied potentials after approximately 80 min of adsorption.

Upon rinsing with PBS, a small rapid increase in the frequency was observed for both oxide types and the different applied potentials, followed by a stabilization as shown in Figure 9a. The dissipation decreased slightly, as shown in Figure 9b. This means that a small amount of molecules was desorbing from the surface. Thus, the adsorption of HEL is a largely irreversible process.

When the adsorption processes of 1 mg/mL of HEL on the electrochemically grown titanium oxide at the different applied potentials in Figure 9a were compared, it was observed that the initial adsorption rate was fastest at OCP, whereas it was slower and similar for 0 and 0.6 V. After approximately 80 min of adsorption, the adsorbed amount of 1 mg/mL of HEL molecules on the electrochemically grown titanium oxide for the different applied potentials was largest for OCP and least for 0.6 V, i.e., −29.1 ± 0.1 and −26.5 ± 0.1 Hz, respectively, as observed in Figure 9a.

DISCUSSION

In general, the simultaneous application on Ti of an anodic potential and adsorption of molecules leads to results that might be hard to interpret because two phenomena are taking place at the same time, i.e., the oxidation of Ti and the adsorption of molecules on the Ti surface. Thus, for adsorption studies with ECQCM-D, development of a method was needed, allowing one to distinguish between both phenomena, or alternatively, precalibaration of one process (oxide growth) so that it can be subtracted from the total signal (oxide growth + biomolecule adsorption).

Characteristics of the Electrochemically Grown TiO$_2$ Film. The oxidation of Ti by means of ECQCM-D showed a decrease in the frequency shift (mass increase) upon application of an anodic potential as shown in Figure 3. As shown by XPS, this decrease in frequency is mainly due to oxygen uptake/oxidation responsible for the growth of the titanium oxide layer (35−41, 75). The chemical composition of the surface oxides mainly consisted of TiO$_2$, with a small percentage of the suboxides Ti$_2$O$_3$ and TiO

present primarily at the metal−oxide interface, as judged from the decrease of these signals with an increase in the oxide thickness and also in line with earlier data from the literature (63, 71, 73). The oxide layer stabilized only after several hours and had a thickness that was proportional to the oxidation potential for values up to 1.8 V. The intensity of the suboxides, i.e., TiO and Ti$_2$O$_3$, decreased by an increase in the oxidation potential, whereas that of the oxide TiO$_2$ increased. Also, no change in the dissipation was observed, which is what is expected for rigid films. A relatively larger frequency shift, and thus a larger relative thickness change of the oxide, was observed when the Ti surface was oxidized at 2.6 V, and the dissipation was no longer stable but decreased. These effects observed at 2.6 V cannot yet be given an unambiguous interpretation but are most likely related to the morphology of the initial Ti film and of the formed oxide film. The initial metal film has a certain roughness, which is not necessarily the same as the roughness of the formed oxide film, and the latter is likely to change with thickness. Furthermore, it is well-known in anodic oxidation that local areas of the film may be subject to breakthrough currents that are then "self-healing" and can give rise to local vertical oxide growth and/or porous oxide. Either of the latter will be sensed with high sensitivity by QCM-D because it measures the total oxygen uptake independently of the location and also senses the water trapped in porous areas. We speculate that these factors qualitatively lie behind the observed phenomena at 2.6 V, but further investigations with transmission electron microscopy morphology studies on the films before and after oxidation are required to provide better mechanistic insight.

Over the whole range of potentials, a good correlation is obtained between the ECQCM-D thickness changes and the estimated XPS thickness of the layer formed by electrochemical oxidation, as illustrated for 1 and 2.6 V in Table 1.

Implications for Biomolecular Adsorption Studies onto TiO$_2$ under an Applied Potential. The results show that, for the present Ti films and buffer solution, oxidation potentials up to 1.8 V are most suitable to oxidize the Ti surface for adsorption studies because the oxide layer was growing proportionally with the applied potential, with a growth rate similar to that of bulk Ti, and the dissipation shift was not changing. The range is likely to be extendable by improved morphology control on the initial Ti film. It is also likely that experiments with a higher potential with simultaneous oxide growth and biomolecular adsorption can be performed, where the precalibrated oxide growth is subtracted. Control whether the biomolecule adsorption affects the oxide growth rate or not can then be done with XPS.

Lysozyme Adsorption onto Ti under an Applied Potential. According to the literature (76, 77), the first rapid adsorption step in Figure 9a,b was attributed to the formation of a rigid, closed-packed monolayer of "side-on" molecules. The following slower adsorption process was assigned to the formation of a more loosely packed second layer, which resulted in a significant increase in dissipation.

When a comparison was made between the adsorption behavior of HEL molecules at OCP on the Ti-coated QCM crystals, covered with either its native oxide or an electrochemically grown oxide layer, no significant differences were observed. Thus, small changes of the thickness of the oxide layer did not affect the adsorption behavior of 1 mg/mL of HEL at OCP. It was also found that the adsorption behavior of HEL on an electrochemically grown titanium oxide film for the different applied potentials was similar to its adsorption behavior on a Ti surface, covered with its native oxide layer.

Because the monitored dissipation shifts for 1 mg/mL of HEL adsorption, as listed in Table 2, were much smaller than 10^{-5} (57), the Sauerbrey equation was valid. Therefore, the Sauerbrey equation was used to determine the adsorbed amounts per unit area. The results for the adsorbed amounts per unit area for 1 mg/mL of HEL, as listed in Table 2, were compared with the adsorbed amounts found in other QCM studies of lysozyme adsorption in the literature. Vörös (78) investigated the adsorption of 80 μg/mL of HEL on TiO_2. An adsorbed amount at a saturation of approximately 350 ng/cm^2 was found. Our results for the adsorbed amounts per unit area were significantly larger than this value. This difference can most likely be attributed to the difference in the HEL concentration.

CONCLUSIONS

The first goal was to prepare Ti substrates suitable for biomolecular adsorption studies under applied potential. With ECQCM-D, vapor-deposited Ti films on quartz crystals were oxidized at different anodic potentials. A stable oxide layer was obtained after application of an oxidation potential for several hours. The Ti films exhibited a growth rate for the oxide of around 2.5–3 nm/V. A good correlation was obtained between the ECQCM-D results and the XPS depth profiles for the different oxidized Ti films. XPS showed that the chemical composition of the surface oxide was mainly TiO_2, with a small percentage of Ti_2O_3 and TiO present primarily at the oxide–metal interface. With increasing potential, the intensity of Ti_2O_3 and TiO decreased because of the growing TiO_2 layer.

A successful preparation of Ti films with a predefined electrochemically grown oxide, deposited on quartz crystals, was achieved for investigations on the influence of an electric field on the adsorption of biomolecules. This means that, upon adsorption of molecules on the polarized Ti surface, the frequency and dissipation shift will only be attributed to the formation of the adsorbed layer of molecules. The results of this study show that the combination of QCM-D with electrochemical measurements is a valuable technique when one wants to control the oxide layer thickness for biomolecule adsorption studies under the influence of external fields.

Once a stable titanium oxide film was obtained, the second goal was the investigation of the adsorption behavior of HEL under applied potential. No significant interdependence of the adsorption of HEL and the applied potential was observed. This implied that the adsorption behavior of HEL was not influenced by the applied potential on the electrochemically grown titanium oxide layer. However, because this adsorption study was only a first one, further research is necessary to fully understand the effect of the applied potential on the adsorption behavior of HEL and other biomolecules.

This study shows that the experimental methodology used to perform protein adsorption experiments under applied potential by means of ECQCM-D makes the quantification of protein adsorption on oxidized Ti under applied potential possible. It also gives insight in the viscoelastic properties of the adsorbed protein layer by measurement of the dissipation of the system.

REFERENCES AND NOTES

(1) Kasemo, B.; Lausmaa, J. *Crit. Rev. Biocompat.* **1986**, *2* (4), 335–380.
(2) Kasemo, B. *J. Prosthet. Dent.* **1983**, *49*, 832–837.
(3) Kasemo, B.; Lausmaa, J. In *Tissue-Integrated Prostheses. Osseointegration in Clinical Dentistry*; Brånemark, P.-I., Zarb, G. A., Albrektsson, T., Eds.; Quintessence: Chicago, 1985; p 99.
(4) Andrade, J. D. *Surface and Interfacial Aspects of Biomedical Polymers*; Plenum Press: New York, 1985.
(5) Puleo, D. A.; Nanci, A. *Biomaterials* **1999**, *20* (23−24), 2311–2321.
(6) Ratner, B. D.; Castner, D. G.; Horbett, T. A.; Lenk, T. J.; Lewis, K. B.; Rapoza, R. J. *J. Vac. Sci. Technol. A* **1990**, *8* (3), 2306–2317.
(7) Brunette, D. M.; Tengvall, P.; Textor, M.; Thomsen, P. *Titanium in Medicine: Material Science, Surface Science, Engineering, Biological Responses and Medical Applications*; Springer-Verlag: Berlin, 2001.
(8) Ratner, B. D.; Hoffman, A. S.; Schoen, F. J.; Lemons, J. E. *Biomaterials Science. An Introduction to Materials in Medicine*, 2nd ed.; Academic Press: San Diego, 2004.
(9) Brusatori, M. A.; Tie, Y.; Van Tassel, P. R. *Langmuir* **2003**, *19* (12), 5089–5097.
(10) Khan, M. A.; Williams, R. L.; Williams, D. F. *Biomaterials* **1996**, *17* (22), 2117–2126.
(11) Khan, M. A.; Williams, R. L.; Williams, D. F. *Biomaterials* **1999**, *20* (7), 631–637.
(12) Khan, M. A.; Williams, R. L.; Williams, D. F. *Biomaterials* **1999**, *20* (8), 765–772.
(13) Salt, D. *Hy-Q Handbook of Quartz Crystal Devices*; Van Nostrand Reinhold Co. Ltd.: Padstow, Cornwall, U.K., 1987.
(14) Kasemo, B.; Törnqvist, E. *Phys. Rev. Lett.* **1980**, *44* (23), 1555–1558.
(15) Kösslinger, C.; Uttenthaler, E.; Drost, S.; Aberl, F.; Wolf, H.; Brink, G.; Stanglmaier, A.; Sackmann, E. *Sens. Actuators, B* **1995**, *24* (1−3), 107–112.
(16) Caruso, F.; Furlong, D. N.; Kingshott, P. *J. Colloid Interface Sci.* **1997**, *186* (1), 129–140.
(17) Höök, F.; Rodahl, M.; Kasemo, B.; Brzezinski, P. *Proc. Natl. Acad. Sci. U.S.A.* **1998**, *95* (21), 12271–12276.
(18) Thompson, M.; Arthur, C. L.; Dhaliwal, G. K. *Anal. Chem* **1986**, *58* (6), 1206–1209.
(19) Höök, F.; Rodahl, M.; Brzezinski, P.; Kasemo, B. *Langmuir* **1998**, *14* (4), 729–734.
(20) Rodahl, M.; Höök, F.; Kasemo, B. *Anal. Chem* **1996**, *68* (13), 2219–2227.
(21) Rodahl, M.; Kasemo, B. *Rev. Sci. Instrum.* **1996**, *67* (9), 3238–3241.
(22) Fredriksson, C.; Kihlman, S.; Rodahl, M.; Kasemo, B. *Langmuir* **1998**, *14* (2), 248–251.
(23) Keller, C. A.; Kasemo, B. *Biophys. J.* **1998**, *75* (3), 1397–1402.

(24) Steinem, C.; Janshoff, A.; Wegener, J.; Ulrich, W. P.; Willenbrink, W.; Sieber, M.; Galla, H. J. *Biosens. Bioelectron.* **1997**, *12* (8), 787–808.

(25) Rodahl, M.; Höök, F.; Krozer, A.; Brzezinski, P.; Kasemo, B. *Rev. Sci. Instrum.* **1995**, *66*, 3924–3930.

(26) Bearinger, J. P.; Vörös, J.; Hubbell, J. A.; Textor, M. *Biotechnol. Bioeng.* **2003**, *82* (4), 465–473.

(27) Brusatori, M. A.; Van Tassel, P. R. *Biosens. Bioelectron.* **2003**, *18* (10), 1269–1277.

(28) Kurrat, R.; Walivaara, B.; Marti, A.; Textor, M.; Tengvall, P.; Ramsden, J. J.; Spencer, N. D. *Colloid Surf. B* **1998**, *11* (4), 187–201.

(29) Tiefenthaler, K.; Lukosz, W. *J. Opt. Soc. Am. B* **1989**, *6* (2), 209–220.

(30) Azzam, R. M.; Bashara, N. M. *Ellipsometry and Polarized Light*; North Holland Physics Publishing: Amsterdam, The Netherlands, 1987.

(31) Vroman, L.; Lukosevicius, A. *Nature* **1964**, *204* (495), 701–703.

(32) Höök, F.; Vörös, J.; Rodahl, M.; Kurrat, R.; Böni, P.; Ramsden, J. J.; Textor, M.; Spencer, N. D.; Tengvall, P.; Gold, J.; Kasemo, B. *Colloid Surf. B* **2002**, *24*, 155–170.

(33) Hibbert, D. B.; Weitzner, K.; Tabor, B.; Carter, P. *Biomaterials* **2000**, *21* (21), 2177–2182.

(34) Cosman, N. P.; Roscoe, S. G. *Anal. Chem* **2004**, *76* (19), 5945–5952.

(35) Bourdet, P.; Vacandio, F.; Argeme, L.; Rossi, S.; Massiani, Y. *Thin Solid Films* **2005**, *483* (1−2), 205–210.

(36) Eickes, C.; Rosenmund, J.; Wasle, S.; Doblhofer, K.; Wang, K.; Weil, K. G. *Electrochim. Acta* **2000**, *45* (22−23), 3623–3628.

(37) Jerkiewicz, G.; Vatankhah, G.; Lessard, J.; Soriaga, M. P.; Park, Y. S. *Electrochim. Acta* **2004**, *49* (9−10), 1451–1459.

(38) Olsson, C. O. A.; Vergé, M. G.; Landolt, D. *J. Electrochem. Soc.* **2004**, *151* (12), B652–660.

(39) Tian, M.; Pell, W. G.; Conway, B. E. *Electrochim. Acta* **2003**, *48* (18), 2675–2689.

(40) Vergé, M. G.; Olsson, C. O. A.; Landolt, D. *Corros. Sci.* **2004**, *46* (10), 2583–2600.

(41) Vergé, M. G.; Mettraux, P.; Olsson, C. O. A.; Landolt, D. *J. Electroanal. Chem.* **2004**, *566* (2), 361–370.

(42) Fleming, B. D.; Praporski, S.; Bond, A. M.; Martin, L. L. *Langmuir* **2008**, *24* (1), 323–327.

(43) Imoto, T.; Johnson, L.; North, A.; Phillips, D.; Rupley, J. In *The Enzymes*, 3rd ed.; Boyer, P. D., Ed.; Academic Press: New York, 1972; Vol. 7, p 665.

(44) Gölander, C.-G.; Hlady, V.; Caldwell, K.; Andrade, J. D. *Colloid Surf.* **1990**, *50*, 113–130.

(45) Janshoff, A.; Galla, H.-J.; Steinem, C. *Angew. Chem., Int. Ed.* **2000**, *39*, 4004–4032.

(46) Sauerbrey, G. *Z. Phys.* **1959**, *155* (2), 206–222.

(47) Moulder, J. F.; Stickle, W. F.; Sobol, P. E.; Bomben, K. D. *Handbook of X-ray Photoelectron Spectroscopy*; Physical Electronics, Inc.: Chanhassen, MN, 1995.

(48) Seah, M. P. *Practical Surface Analysis by AES and XPS*; Wiley: Chichester, U.K., 1990.

(49) Shirley, D. *Phys. Rev. B* **1972**, *5*, 4709–4714.

(50) Briggs, D.; Grant, J. *Surface Analysis by Auger and X-ray Photoelectron Spectroscopy*; Cromwell Press: Trowbridge, U.K., 2003.

(51) Stickle, W. F.; Sobol, P. E. *Surf. Interface Anal.* **1992**, *19* (1−12), 165–170.

(52) Lausmaa, J. *J. Electron Spectrosc.* **1996**, *81* (3), 343–361.

(53) Aladjem, A. *J. Mater. Sci.* **1973**, *8* (5), 688–704.

(54) Kuromoto, N. K.; Simão, R. A.; Soares, G. A. *Mater. Charact.* **2007**, *58* (2), 114–121.

(55) Marino, C. E.; de Oliveira, E. M.; Rocha, R. C.; Biaggio, S. R. *Corros. Sci.* **2001**, *43* (8), 1465–1476.

(56) Schultze, J. W.; Lohrengel, M. M. *Electrochim. Acta* **2000**, *45* (15−16), 2499–2513.

(57) Voinova, M. V.; Rodahl, M.; Jonson, M.; Kasemo, B. *Phys. Scr.* **1999**, *59*, 391–396.

(58) Marsh, J.; Gorse, D. *Electrochim. Acta* **1998**, *43* (7), 659–670.

(59) Ohtsuka, T.; Masuda, M.; Sato, N. *J. Electrochem. Soc.* **1985**, *132* (4), 787–792.

(60) Lausmaa, J.; Kasemo, B.; Mattsson, H. *Appl. Surf. Sci* **1990**, *44* (2), 133–146.

(61) Lausmaa, J.; Kasemo, B. ; Rolander, U.; Bjursten, L. M.; Ericson, L. E.; Rosander, L.; Thomsen, P. In *Surface Characterization of Biomaterials*; Ratner, B. D., Ed.; Elsevier Science Publishers BV: Amsterdam, The Netherlands, 1988; p 161.

(62) Marino, C. E. B.; Nascente, P. A. P.; Biaggio, S. R.; Rocha, R. C.; Bocchi, N. *Thin Solid Films* **2004**, *468* (1−2), 109–112.

(63) Milosev, I.; Metikos-Hukovic, M.; Strehblow, H. H. *Biomaterials* **2000**, *21* (20), 2103–2113.

(64) Vesel, A.; Mozetic, M.; Kovac, J.; Zalar, A. *Appl. Surf. Sci.* **2006**, *253* (5), 2941–2946.

(65) Lu, F. H.; Chen, H. Y. *Surf. Coat. Technol.* **2000**, *130* (2−3), 290–296.

(66) Mayer, J. T.; Diebold, U.; Madey, T. E.; Garfunkel, E. *J. Electron Spectrosc.* **1995**, *73* (1), 1–11.

(67) Sodhi, R. N. S.; Weninger, A.; Davies, J. E.; Sreenivas, K. *J. Vac. Sci. Technol. A* **1991**, *9* (3), 1329–1333.

(68) Armstrong, N. R.; Quinn, R. K. *Surf. Sci.* **1977**, *67* (2), 451–468.

(69) Cacciafesta, P.; Hallam, K. R.; Oyedepo, C. A.; Humphris, A. D. L.; Miles, M. J.; Jandt, K. D. *Chem. Mater* **2002**, *14* (2), 777–789.

(70) Halbritter, J.; Leiste, H.; Mathes, H. J.; Walk, P. *Fresenius' J. Anal. Chem.* **1991**, *341* (5−6), 320–324.

(71) Lu, G.; Bernasek, S. L.; Schwartz, J. *Surf. Sci.* **2000**, *458* (1−3), 80–90.

(72) Jeyachandran, Y. L.; Karunagaran, B.; Narayandass, S. K.; Mangalaraj, D.; Jenkins, T. E.; Martin, P. J. *Mater. Sci. Eng., A* **2006**, *431* (1−2), 277–284.

(73) Carley, A. F.; Chalker, P. R.; Riviere, J. C.; Roberts, M. W. *J. Chem. Soc., Faraday Trans. 1* **1987**, *83*, 351–370.

(74) Textor, M.; Sittig, C.; Frauchiger, V.; Tosatti, S.; Brunette, D. M. In *Titanium in Medicine: Material Science, Surface Science, Engineering, Biological Responses and Medical Applications*; Brunette, D. M., Tengvall, P., Textor, M., Thomsen, P., Eds.; Springer-Verlag: Berlin, 2001; p 171.

(75) Tsionsky, V.; Daikhin, L.; Zilberman, G.; Gileadi, E. *Faraday Discuss.* **1997**, *107*, 337–350.

(76) Su, T. J.; Lu, J. R.; Thomas, R. K.; Cui, Z. F.; Penfold, J. *Langmuir* **1998**, *14* (2), 438–445.

(77) Wahlgren, M.; Arnebrant, T.; Lundstrom, I. *J. Colloid Interface Sci.* **1995**, *175* (2), 506–514.

(78) Vörös, J. *Biophys. J.* **2004**, *87*, 553–561.